



Minerva Access is the Institutional Repository of The University of Melbourne

Author/s:

Perera, JS;Lam, N;Disfani, MM;Gad, E

Title:

Experimental and Analytical Investigation of a RC Wall with a Gabion Cushion Subjected to Boulder Impact

Date:

2021-05-31

Citation:

Perera, J. S., Lam, N., Disfani, M. M. & Gad, E. (2021). Experimental and Analytical Investigation of a RC Wall with a Gabion Cushion Subjected to Boulder Impact. INTERNATIONAL JOURNAL OF IMPACT ENGINEERING, 151, <https://doi.org/10.1016/j.ijimpeng.2021.103823>.

Persistent Link:

<https://hdl.handle.net/11343/310876>

16 **Abstract**

17 An experimental investigation involving the use of a full-scale pendulum device to deliver solid
18 object impact on a reinforced concrete (RC) barrier specimen that was fitted with a layer of
19 gabion cushion is reported in this paper. The deflection behaviour of the stem wall of the RC
20 barrier including the tensile strains developed in the longitudinal reinforcement was of interests.
21 Results recorded from the tests are compared with results from control experiments which were
22 without the protection of any cushion materials. The introduction of a layer of cushion is shown
23 to be able to have the contact force reduced by more than 95% and deflection demand reduced
24 by about 70%. An analytical procedure employing the Hunt and Crossley contact model, Swiss
25 code model and two-degrees-of-freedom (2DOF) system modelling technique is presented for
26 calculating the flexural response behaviour of the cushioned barrier and validated by
27 comparison with experimental measurements. An important outcome from the study is a simple
28 hand calculation procedure featuring the use of a closed form expression along with a design
29 chart which is illustrated by a worked example, to facilitate uptake in design practices.
30 **Keywords:** impact action, rockfall, impact barrier, gabion cushion

31 **Acknowledgement**

32 Financial support from the Australian Research Council (ARC) Discovery Project
33 DP170101858 entitled “New Approach for Design of Barriers for Impact” is gratefully
34 acknowledged. This paper is published with the permission of the Head of the Geotechnical
35 Engineering Office and the Director of Civil Engineering and Development, Hong Kong SAR
36 Government.

37 **Notations**

A_{st} = total area of reinforcement at tensile side
 B = wall length
 COR = coefficient of restitution

d	=	distance between compressive surface of concrete and centre of tensile bar
D	=	depth of concrete section
D_l	=	linear damping factor
D_n	=	nonlinear damping factor
e	=	thickness of cushion layer
E	=	Elastic modulus of concrete
EI_{cr}	=	flexural rigidity of cracked concrete
f'_c	=	compressive strength of concrete
f_y	=	tensile strength of reinforcement
F_c	=	contact force
F_{cmax}	=	maximum contact force
h	=	wall height
h_i	=	vertical distance between point of impact and axis of rotation
k	=	stiffness of the target responding within the elastic limit
k_{cr}	=	cracked stiffness
k_l	=	stiffness of frontal spring in linear visco-elastic 2DOF model
k_n	=	stiffness of frontal spring in non-linear visco-elastic 2DOF model
m	=	impactor's mass
m_2	=	combined mass of the wall and cushion
m_{wall}	=	idealised lumped mass representing the reinforced concrete wall
m_{gabion}	=	contributory mass of the cushion
M_E	=	modulus of elasticity of the gabion layer
M_y	=	yield moment capacity of the reinforced concrete wall section
M_u	=	ultimate moment capacity of the reinforced concrete wall section
p	=	exponent characterising the non-linearity of spring
r	=	radius of equivalent sphere
r_1	=	radius of the force transmitted area
T_m	=	time taken for the contact force to rise to its peak
T_{m2}	=	time taken by the target to deflect to the full extent
v_0	=	impact velocity
v_1	=	velocity of the impactor after the impact
v_2	=	velocity of the target after the impact
δ	=	indentation of impactor into surface of target (linear)
δ_{max}	=	maximum indentation
$\dot{\delta}$	=	velocity of indentation
$\dot{\delta}_0$	=	relative velocity between two colliding objects at initial contact
Δ	=	maximum deflection of cantilevered wall
Δ_y	=	deflection of stem wall at yield limit
Δ_{yi}	=	deflection of stem wall at the point of impact at yield limit
γ	=	reduction factor
ρ	=	density of the gabion cushion
ε_s	=	maximum tensile strain of reinforcement
ε_{sy}	=	yield strain of reinforcement

ϕ	=	bending curvature of the reinforced concrete wall
ϕ_y	=	yield curvature of the reinforced concrete wall
ϕ_k	=	internal friction angle of particles
λ	=	ratio of the target mass to the impactor mass
λ_2	=	ratio of the combined target mass to the impactor mass

38 **1 Introduction**

39 Dwellings built in mountainous areas can be vulnerable to rockfall and landslide hazards. In
 40 areas that are subject to such hazards including many parts of Switzerland, France, Italy, Japan
 41 and some overly congested metropolitan areas across Asia (e.g. Hong Kong) protective
 42 structures such as earth dams, rockfall sheds and reinforced concrete (RC) barriers have been
 43 erected to provide protection. Earth dams are massive, intrusive and require ample accessible
 44 space to build thereby posing safety issues in mountainous areas. RC barriers and rockfall sheds
 45 occupy much less space than earth dams but require a layer of materials to be placed on surfaces
 46 that are exposed to impact by boulders to function as “cushion”. For example, rockfall sheds
 47 (that are commonly found in mountainous roadways in Switzerland) are typically covered by a
 48 layer of gravel to cushion the impact of falling rocks [1].

49 Gabions are rectangular steel cages made of hexagonal double twisted wire mesh or square
 50 welded wire mesh filled with appropriately sized rock particles and then stacked in front of a RC
 51 barrier to provide additional protection. The effectiveness of the gabion cushion layer in
 52 enhancing the impact-resistant capacity of a barrier has been investigated in Refs. [2-4]. This
 53 cushion layer is normally designed to reduce the intensity of the contact pressure that is
 54 potentially generated by the impact of a falling boulder in view of the risks of the RC protective
 55 slab/barrier being punched through at the point of contact [5-8]. In addition to controlling the
 56 contact pressure, the cushion layer also mitigates impulsive action transmitted to the barrier [9].

57 There are number of experimental studies available in the literature on the effectiveness of the
 58 gabion cushion layer. Some of these experimental arrangements used a soil embankment as the
 59 structural component [2, 3] and some used a concrete wall as the structural element [4]. In an

60 investigation reported in Ref. [10] several layers of gabions made up of different materials
61 (forming a sandwich structure) were offered as a promising technical solution for countering
62 rockfall hazards. However, Improvements to the flexural performance behaviour of the structure
63 resulted from the transmitted impulsive action have never been considered. Recognising this
64 knowledge gap, the authors performed a full-scale test on RC barrier specimen. The cantilevered
65 RC wall was impact tested by a pendulum device. Full-scale unconfined compression testings of
66 the gabion were also performed alongside impact experiments to characterise the properties of
67 the gabion. Influence by the type of infill and cage strengths have also been studied. In addition
68 to studying the contact force behaviour, the experimental investigation was also aimed at
69 quantifying the influence of the gabion cushion on the deflection demand of the stem wall
70 resulted from the impulsive action. Barriers that are with, and without, protection by gabions
71 were tested to compare their respective contact force, deflection demand and reinforcement
72 strains generated by the impact.

73 Alongside the impact experiments, an analytical procedure for guiding the structural design of
74 RC rockfall barriers that are protected by gabions has also been derived. The development of the
75 analytical methodology involved a two-degree-of-freedom (2DOF) spring connected lumped
76 mass model featuring the use of the Hunt and Crossley model (to define the hysteretic properties
77 of the frontal spring representing the cushioning action of the gabions). The forcing function of
78 the impact and the resulting deflection of the stem wall can be predicted using the analytical
79 model which was then validated by experimental measurements from full scale testings. A hand
80 calculation procedure based on displacement principles is introduced at the end of the article,
81 illustrated with a worked example. The procedure involves the use of a design chart to facilitate
82 determination of the cushion reduction factor.

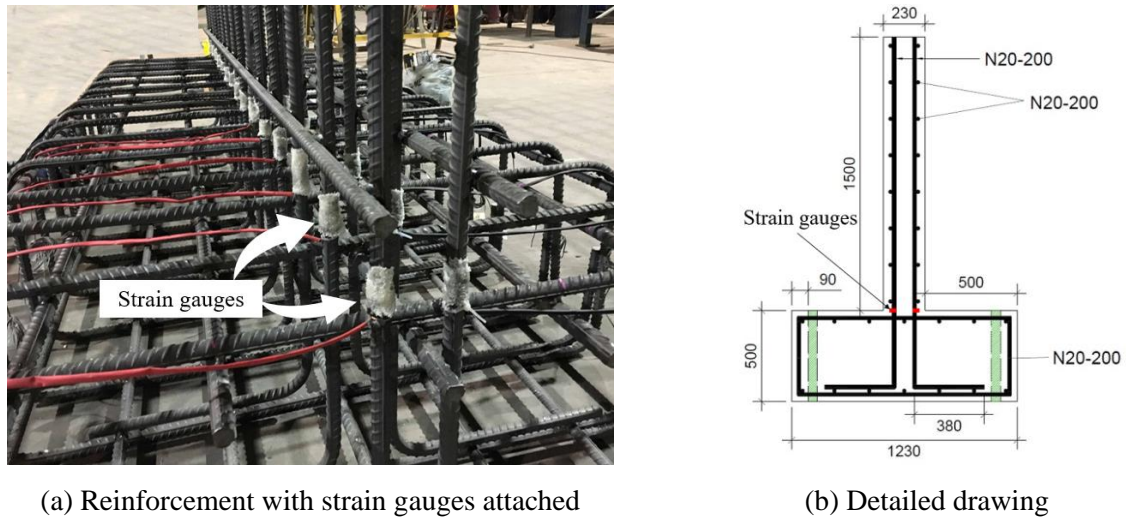
83 **2 Full Scale Horizontal Impact Tests**

84 In practice RC barriers vary in size considerably depending on site conditions and the nature of
85 the rockfall hazard. The decision made on the dimensions of the barrier specimen that was
86 tested by the authors was to ensure that the manner of casting the wall and the type of materials
87 used were consistent with that of a real RC barrier. The stem wall of the test barrier was 230
88 mm thick and 1.5 m tall and was reinforced with 20 mm diameter reinforcing bars with 40 mm
89 cover. These dimensions were sufficiently large to fulfill the stated criterion. The length of the
90 barrier was selected as twice the height of the wall (which is 3 m) and the rationale behind the
91 selection of this length is explained under Section 4.3. A second model barrier is presented in
92 Appendix A as worked example to illustrate the proposed calculation methodology is of a much
93 larger dimension. In view of the frequent occurrences of impact by boulders the test specimen
94 was designed not to surpass the yield limit.

95 The RC wall was cast on a base slab of 0.5 m thick and 1.23 m long. Grade D500N, 15 tensile
96 and 15 compressive reinforcing steel bars were used as vertical and horizontal reinforcement in
97 the cantilevered wall (Fig. 1). Similar reinforcement arrangement was used for the base slab to
98 ensure that the cantilevered wall was fixed rigidly to the foundation which was in turn held
99 firmly onto the strong floor of the laboratory. Strain gauges for high elongation strain
100 measurements in post yield conditions were attached to the base of the wall (refer Fig. 1 for the
101 exact location) on each vertical steel bars prior to the casting of the concrete; 30 strain gauges
102 were deployed in total to instrument the test wall (15 on each side). Data recorded from the
103 strain gauges were acquired at a rate of 2 kHz during cyclic stress reversals.

104 The test wall was cast of concrete with maximum aggregate size of 20 mm, characteristic (28
105 days) compressive strength exceeding 40 MPa and density of 2400 kg/m³ approximately.
106 Compression tests were carried out on six concrete cylinders during the time the impact tests
107 were carried out. Cylinders were tested in different time intervals (after 28 days, 2 days before

108 the beginning of the test and two weeks after the test). The concrete strength was found to not
109 vary significantly across the six tests, and the test results averaged at 47 MPa.



(a) Reinforcement with strain gauges attached

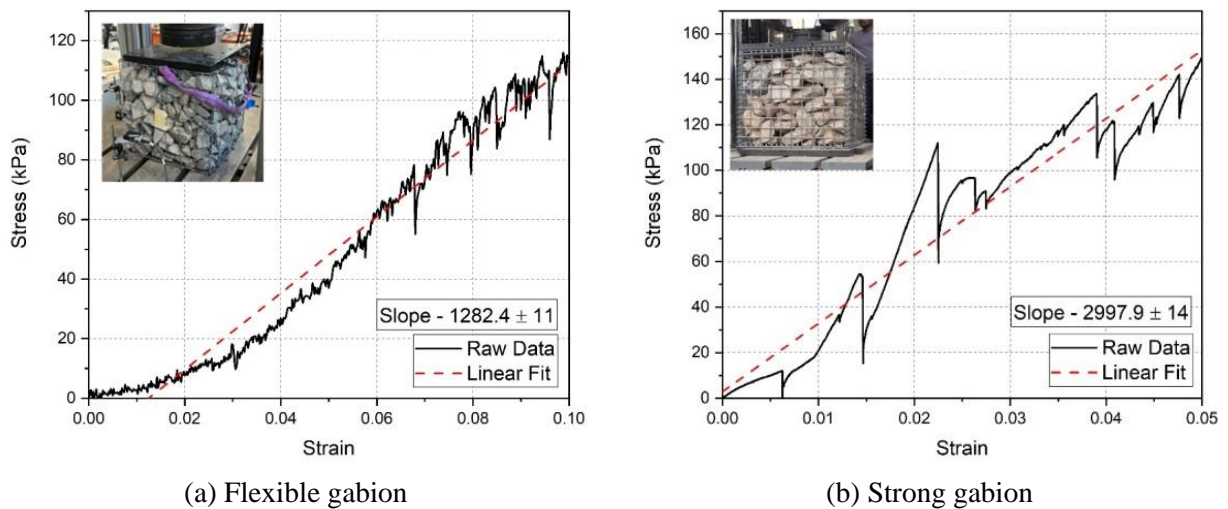
(b) Detailed drawing

110 **Fig. 1 Details of the reinforced concrete wall**

111 Typical size of a gabion box could vary from 500 mm to 1000 mm along the width and 500 mm
112 to 2000 mm along the length directions. The gabions selected for this experiment were cubical
113 in shape and with side dimensions of 500 mm. Any stone or other material may be used to fill
114 the gabion but to ensure the durability of the structure the infill material must be durable,
115 sufficiently hard, weather-resistant, non-friable and insoluble. The most used materials are river
116 stones or quarried stones. The most appropriate size for infill stone varies from 1 and 1.5 to 2
117 times the dimension of the opening of the mesh to prevent losses of material [11]. Two types of
118 infill materials: crushed gravel (70 - 100 mm) and river pebbles (50 - 200 mm) were used in this
119 test. The relatively flexible gabion cages had wire mesh of 3 mm in diameter (with 75 mm
120 square openings) whereas stronger cages had wire mesh of 5 mm in diameter (with 50 mm
121 square openings).

122 The average gabion box weighted 210 kg and 215 kg for crushed gravel and river pebbles fills,
123 respectively. The bulk density of a gabion box was accordingly 1451 kg/m³ for a gravel filled
124 gabion and 1486 kg/m³ for river pebbles filled gabion. Static tests in unconfined conditions were
125 carried out on specimens of the gabion boxes to obtain their stiffness properties. The test results

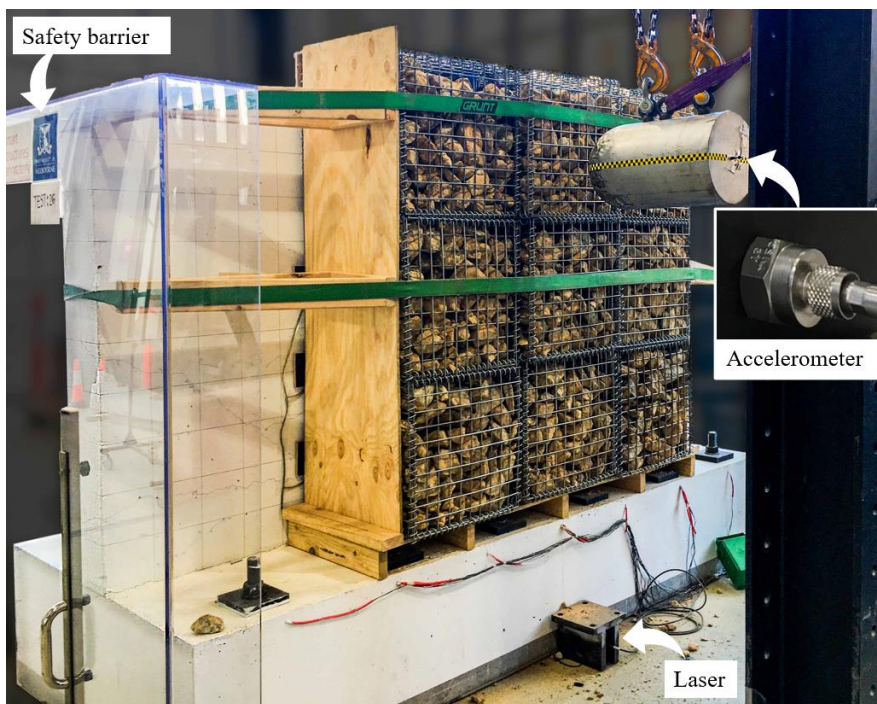
126 are expressed in terms of the modulus of elasticity. Each gabion box was loaded quasi-statically
 127 by an actuator which was rated at 1 MN (MTS 311.31) as shown in Fig. 2. A 32 mm thick steel
 128 plate was placed on top of the gabion box to distribute the compressive force evenly on its upper
 129 surface. Compression strains of up to 0.2 were applied at a rate of 1 mm/s. Two tests were
 130 conducted for each type of fill materials for the flexible gabions, and four tests for each type of
 131 fill materials for the stronger gabions. Modulus of elasticity (M_E) of the gabions was inferred
 132 from test results based on the average slope of the stress-strain diagram as illustrated in Fig. 2.
 133 The compressive stiffness of the gabion box was mainly dependant on the strength of the box.
 134 With flexible gabions an average M_E value of 1172 kPa was recorded. With the stronger gabions
 135 a higher M_E value of 2985 kPa was recorded. For calculation purposes the value of M_E was
 136 rounded up to 1200 kPa for the flexible gabions and 3000 kPa for the stronger gabions.



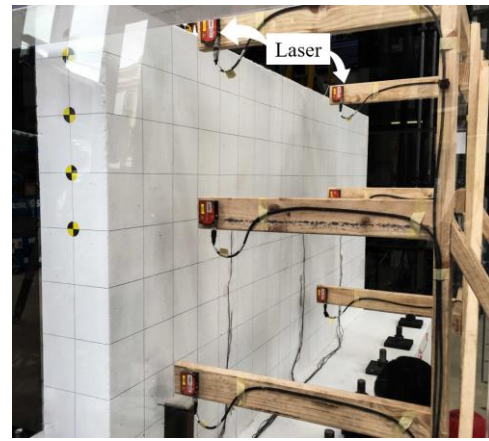
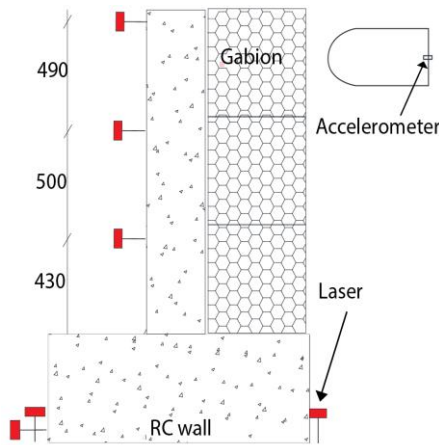
137 **Fig. 2 Unconfined compression test**

138 In the full-scale impact test setup, nine gabions were placed in a 3 by 3 matrix which was
 139 surrounded by a frame made of 17 mm thick plywood for holding the gabions in position. A
 140 plywood stage was used at the base to prevent any contact of the gabions with the threaded rods
 141 that were used to hold the base slab down onto the strong floor of the laboratory. The frame and
 142 gabions were then secured to the cantilevered wall using truck lashing belts. A photograph
 143 displaying an overview of the test set-up including the RC wall specimen, gabion cushion layer,
 144 the impactor object and details of the instrumentation is shown in Fig. 3.

145 Three “torpedo” shaped impactors weighing 280 kg, 435kg and 1020 kg (for impactor “1”, “2”
146 and “3” respectively) were made of solid steel and had their “contact end” (the end for striking
147 the target) machined into a hemispherical surface (with diameters 150 mm, 150 mm and 200
148 mm respectively). An accelerometer (Model: 3200B6M by Dytran) with measurement capacity
149 of up to 2500 g was screwed onto the flat end of the steel impactor to record its acceleration
150 time-history (Fig 3 (a)). The amount of contact force generated by the impact could then be
151 calculated. The accelerometer had frequency response of up to 10 kHz. A high-speed camera
152 (model Phantom v2512) was used to capture images taken at the location of contact, and to
153 record the velocity of the impactor at all stages of the impact from initial contact through to re-
154 bounce. Model ILD 1302 laser sensors (Micro-Epsilon) with measurement frequency of up to
155 750 Hz were employed for capturing the motion of the test wall. Laser sensors were attached to
156 a timber frame to take measurements at the following locations on the rear face of the test wall
157 at the centreline and at the edge: (i) close to the upper edge, (ii) at two-thirds height, (iii) at one-
158 third height and (iv) close to the ground surface (Fig. 3 (c)). Additional laser sensors were used
159 to detect movement, if any, of the base slab (Fig. 3 (b)).



(a) Front side of the test set up



(b) Details of the instruments

(c) Side view of the set up

160

Fig. 3 Overview of the test set up

161 Four impact experiments were carried out initially as control experiments featuring the use of a
 162 protective steel plate (dimensions: 500 mm x 500 mm x 32 mm) which was attached to the stem
 163 wall at the location where the impactor was to strike (i.e. 150 mm below the upper end of the
 164 wall at the centreline). The protective plate was installed to ensure that the bending behaviour of
 165 the wall was comparable across multiple tests without being distorted by cumulative localised
 166 damage surrounding the point of contact. A total of nine impact experiments were conducted on
 167 the test wall which was protected by the gabion cushion. The point of impact was remained at
 168 the same height. The specimen experienced well distributed crack formation in order that its
 169 behaviour was consistently in a fully cracked state across all the tests. Crack distribution was
 170 monitored following every strike to ensure that no new cracks were formed when subject to
 171 subsequent strikes.

172 Solid steel impactors were lifted, and released, in separate tests to strike the gabion protected
 173 wall specimen. Details of the test setup in relation to the gabion cage, fill materials, impactor
 174 mass, drop height and impact energy are listed in Table 1. Test results including contact force,
 175 maximum deflection (measured by the laser pointing at the centerline closer to the upper edge of
 176 the wall) and maximum strain (measured at the middle of the wall) is also shown on the same
 177 table. Note that [Test C1, 1, 3 and 5], [Test C2, 2, 4 and 6], [Test C3 and 7] and [Test C4 and 8]
 178 were comparable in terms of the amount of energy delivered by the strike. Test 9 which had a

179 much higher energy demand (10 kJ) was performed to highlight the importance of installing a
 180 layer of gabions to protect a RC barrier in a real rockfall scenario.

181 **Table 1 details of the full-scale test sequence**

Test No.	Details of the gabion cage	Impactor mass (kg)	Height of Release (m)	Impact Energy (J)	Contact Force (kN)	Maximum Deflection (mm)	Maximum Strain
C1	No cushion – control experiment	280	1.4	3846	1490	11.7	0.00190
C2	No cushion – control experiment	435	0.58	<u>2471</u>	<u>1110</u>	<u>12.3</u>	<u>0.00210</u>
C3	No cushion – control experiment	280	0.5	<i>1374</i>	<i>920</i>	<i>4.9</i>	<i>0.00100</i>
C4	No cushion – control experiment	435	0.32	1374	800	9.2	0.00160
1	Flexible cage – crushed gravel	280	1.4	3846	19.2	1.9	0.00024
2	Flexible cage – crushed gravel	435	0.58	<u>2471</u>	<u>15.8</u>	<u>1.3</u>	<u>0.00018</u>
3	Flexible cage – pebbles	280	1.4	3846	NA	2.5	0.00035
4	Flexible cage – pebbles	435	0.58	<u>2471</u>	<u>15.2</u>	<u>1.4</u>	<u>0.00019</u>
5	Strong cage – crushed gravel	280	1.4	3846	32	4.0	0.00068
6	Strong cage – crushed gravel	435	0.58	<u>2471</u>	<u>27</u>	<u>3.0</u>	<u>0.00050</u>
7	Strong cage – crushed gravel	280	0.5	<i>1374</i>	<i>15</i>	<i>1.7</i>	<i>0.00027</i>
8	Strong cage – crushed gravel	435	0.32	1374	12.5	1.7	0.00021
9	Strong cage – crushed gravel	1020	1	<u>10006</u>	<u>64</u>	<u>5.5</u>	<u>0.00100</u>

182 One important finding of this full-scale test is that the peak contact force has been reduced
 183 significantly by the extra gabion cushion protection. It was found from deflection measurements
 184 of the wall that the use of gabion cushion has achieved some 50% to 90% reduction of the
 185 deflection of the wall. Same observations were reflected in the strain measurements as well
 186 which is of interest to the design engineer. It was also noticed that the stiffness properties of the
 187 gabion cushion (quantified through the unconfined compression test) has influenced not only the
 188 contact force, but also the deflection demand and tensile strain demand on the RC stemwall.

189 3 Modelling of the Contact Force

190 3.1 Existing Empirical Models for predicting contact force

191 A simple calculation procedure for predicting contact force generated by the impact of a fallen
192 rock was proposed by Ng, Choi, Su, Kwan and Lam [4]. Their analysis was based on the Hertz
193 elastic theory as summarized herein. The impact between a sphere of radius ‘ r ’ and a plane
194 surface can be calculated based on the Hertz contact theory assuming elastic behaviour as shown
195 by Eq. (1) [12]. The main drawback with the presented formulation was the misuse of Hertz law
196 in Ref [14] as Hertz law should only be applicable where materials of the colliding objects are in
197 the elastic state.

$$F_{cmax} = \frac{4E}{3} r^{\frac{1}{2}} (\delta_{max})^{\frac{3}{2}} \quad (1)$$

198 where E is the effective modulus of elasticity (in Pa) and can be taken as the modulus of
199 elasticity of the cushion (M_E) when the stiffness of the cushion layer is significantly lower than
200 that of the impactor. Maximum elastic indentation (δ_{max}) can be estimated using Eq. (2).

$$\delta_{max} = \left(\frac{15mv_0^2}{16Er^{\frac{1}{2}}} \right)^{\frac{2}{5}} \quad (2)$$

201 Substitution of Eq. (2) into Eq. (1) results in Eq. (3).

$$F_{cmax} = 1.25M_E^{\frac{2}{5}} r^{\frac{1}{5}} m^{\frac{3}{5}} v_0^{\frac{6}{5}} \quad (3)$$

202 The main drawback of the presented formulation is that the effect of thickness of the cushion on
203 the contact force has not been taken into account in the derivation of the expressions. There are
204 contact force models available in the literature which consider the effect of thickness of the
205 cushion layer and a comparison of the applicability of those models with the gabion cushion is
206 studied by the author as given in Ref [13]. The empirical formula of Eq. (4) for estimating
207 maximum contact force (F_{cmax}) as stipulated by the Swiss code [14] was found to be most

208 accurate and has a form similar to Eq. (3) with two additional terms namely the thickness of the
209 cushion layer (e) and the friction angle of the gabion fill ($\tan\phi_k$).

$$F_{cmax} \sim 2.8 \times e^{-0.5} \times r^{0.7} \times M_E^{0.4} \times \tan\phi_k \times \left(\frac{mv_0^2}{2}\right)^{0.6} \quad (4)$$

210 Guidelines stipulated in Swiss code [14] were derived from experimental studies performed by
211 Stoffel [15] and numerical analyses undertaken by Bucher [16]. A square-shaped slab of
212 dimensions: 3.4 m \times 3.4 m \times 0.2 m was subject to the impact of a dropped hemispherical
213 shaped steel shell filled with concrete. Three different layers of cushion materials comprised of
214 crushed concrete gravels, alluvial cones and scrap rocks were used to cover the concrete slab. It
215 was revealed from experimental and numerical investigations performed on hemispherical and
216 pyramidal shaped impactor objects that a hemispherical impactor induced higher impact force
217 and less penetration into the surface of the target [17]. Thus, the impact of a piece of rock (with
218 sharp corners) is expected to have lower deflection demand on the wall than what was recorded
219 from tests when other parameters were kept unchanged. Design methods developed using a
220 hemispherical shaped impactor object for cushioned impact is therefore conservative.

221 The modulus of subgrade reaction (M_E) in Eq. (3) and Eq. (4) is the key stiffness parameter for
222 input into the formulae. In the Swiss code both M_E and the internal friction angle $\tan\phi_k$ are
223 used as input parameters to characterise the mechanical properties of the cushion material. Plate
224 bearing test is recommended by Swiss Code [14] and Stoffel [15] for obtaining the value of M_E
225 experimentally. A M_E value of 3200 kPa is recommended for a layer of gravel by Labiouse,
226 Descoedres and Montani [18], and this was essentially the same experiment used for
227 developing the Swiss code guidelines. No recommendation has been reported in the literature
228 for predicting the value of M_E for a gabion cage that contains gravel in a confined condition.
229 The level of compaction that could be achieved in the gabion could influence the value of M_E
230 and much depends on the infill particle properties, steel wire mesh properties and filling
231 methods. To obtain a more reliable estimate for the value of M_E it is recommended to conduct

232 static tests on a single box of gabion as explained in the previous section (in the form of an
233 unconfined compression test) in order that specific properties of the gabion can be taken into
234 account. The higher the assumed value of M_E the higher the predicted contact force value. A
235 large number of static tests on full scale gabion specimens performed by Agostini [11] has
236 contributed to the development of a design chart for obtaining the stress-strain relationship of a
237 gabion. According to the test results, the value of M_E (modulus of elasticity) varied from 1000
238 kPa to 4000 kPa for unconfined conditions and about double the value for confined conditions
239 [11, 19]. In the absence of static test results to characterise the properties of the gabion, a design
240 chart as presented in Agostini [11] can be used to approximate the value of M_E of the gabion.

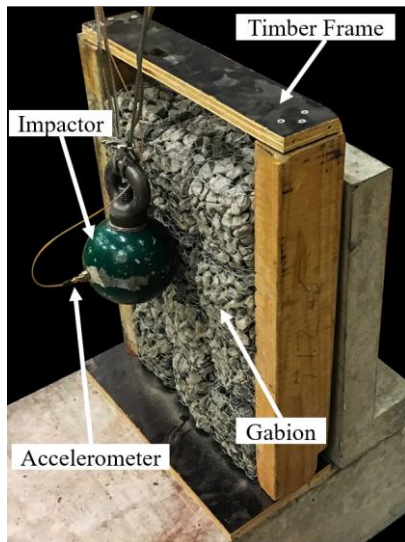
241 The coefficient is empirical in nature and was derived from results obtained from a vast number
242 of drop tests where the layer of gravely particles were well confined [15]. In contrast to the
243 experimental conditions used by Labiouse, Descoeurdes and Montani [18] in deriving Swiss
244 code equation, gabions filled with rock particles cannot be confined when stacked vertically and
245 usually become loose when put in place. The validity of the Swiss code equations (Eq. (4)) in
246 dealing with horizontal impact (as opposed to vertical impact with “drop testing” as was
247 originally intended) and the influence of the gabion cage were uncertainties to be resolved given
248 the change in confinement as the orientation of the test setup is changed. Therefore, the
249 empirical formular of Eq. (4) would need to be re-evaluated for transverse impact on a vertical
250 stack of gabions.

251 ***3.2 Modification factor to allow for change in orientation***

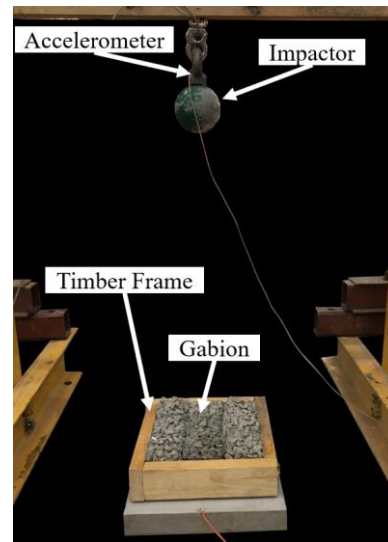
252 Small-scale horizontal and vertical impact tests have been carried out using an array of gabions
253 as shown in Fig. 4 to study the effect of confinement based on the orientation of the setup and
254 the direction of impact. A 2500 g accelerometer (DJB A/123 Ts) which was fixed to the 5kg
255 steel ball impactor was used for measuring the level of shock (de-acceleration) as contact was
256 made with the gabions. The magnitude of contact force generated by the impact was obtained as

257 product of the de-acceleration and mass of the impactor. Gabion boxes were scaled down by 1:5
 258 to be matched with the radius of the impactor. Both the steel wires and filling materials were
 259 scaled by the same factor. A timber frame was used to keep the gabions in place. The recorded
 260 contact force values were then compared and a contact force conversion factor of 0.65 was
 261 found as the impact was changed from vertical to horizontal orientation. The coefficient value of
 262 “0.65” was obtained through calibration against results from the horizontal strike tests on the
 263 gabion cushion. The conversion (reduction) factor so inferred from the comparison of the test
 264 results was used to modify the empirical formular (of Eq. (4)) to allow for change in orientation
 265 of the gabions in a horizontal impact scenario. The modified Eq. (5) is referred herein as the
 266 “Modified Swiss Equation”.

$$F_{cmax} = 0.65 \times 2.8 \times e^{-0.5} \times r^{0.7} \times M_E^{0.4} \times \tan\phi_k \times \left(\frac{mv_0^2}{2}\right)^{0.6} \quad (5)$$



(a) Horizontal pendulum test setup

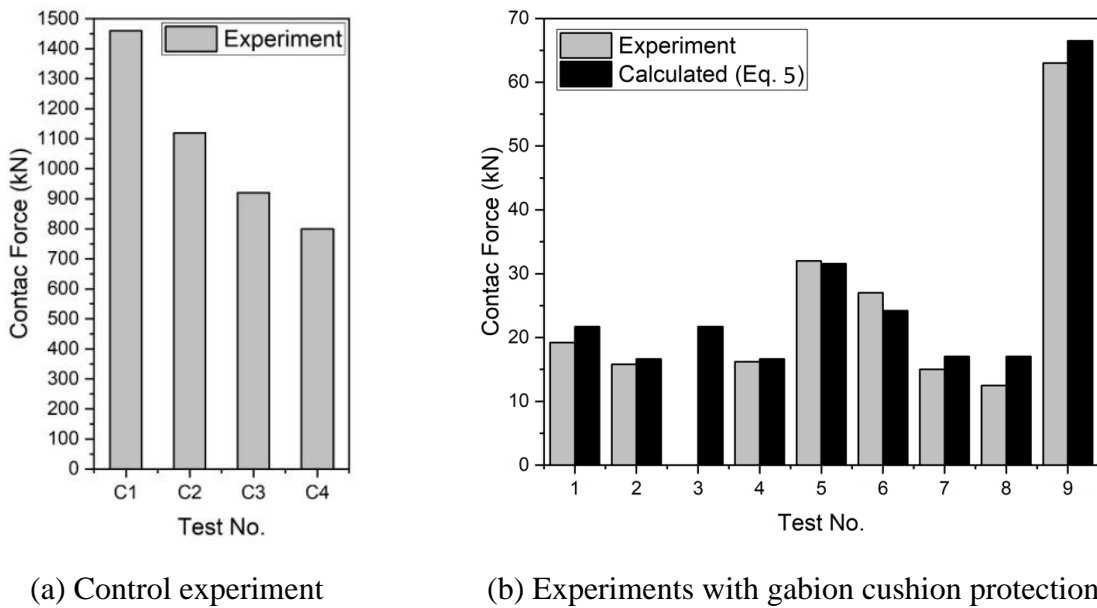


(b) Vertical drop test setup

Fig. 4 vertical and horizontal impact test setups

268 The time-histories of the contact force delivered by the impact (i.e. the forcing function of
 269 impact) for the full-scale impact tests were obtained by multiplying the de-acceleration of the
 270 impactor by its mass. The values of the peak contact force as read off from the measured time-
 271 histories were then compared with predictions obtained from Eq. (5) demonstrating good
 272 consistencies as shown by Fig. 5 (b). These results presented further validates the accuracy of

273 the adopted reduction factor in full scale. Note that the data recorded from Test 3 was discarded
 274 as the measurement device was suspected to be faulty. Peak contact force values recorded from
 275 the control experiments (C1-C4) on a bare wall is also shown in Fig. 5 (a). An order of
 276 magnitude differences can be seen between test results obtained from a bare wall and a
 277 cushioned wall. The cushion layer is shown to have reduced the contact force by more than
 278 95%.



279 **Fig. 5 Comparison of peak contact forces**

280 **4 Modelling of Flexural Response of The RC Wall**

281 The term “*contact force*” refers to the peak contact force which is the maximum force
 282 experienced between the target structure / gabion cushion and the impactor at the point of
 283 contact. Most of the solutions for the peak contact force (as presented in the literature for impact
 284 action without a cushion) give a value of peak force which is transient in nature and can last for
 285 only a very short duration of time to deliver an impulse to the target. The term “*quasi-static*
 286 *force*” refers to the force applied to the target in order to develop the same amount of maximum
 287 deflection that can result from the impact action. This quasi-static force is equivalent to the
 288 product of the stiffness of the target and its maximum deflection resulted from the impact action.

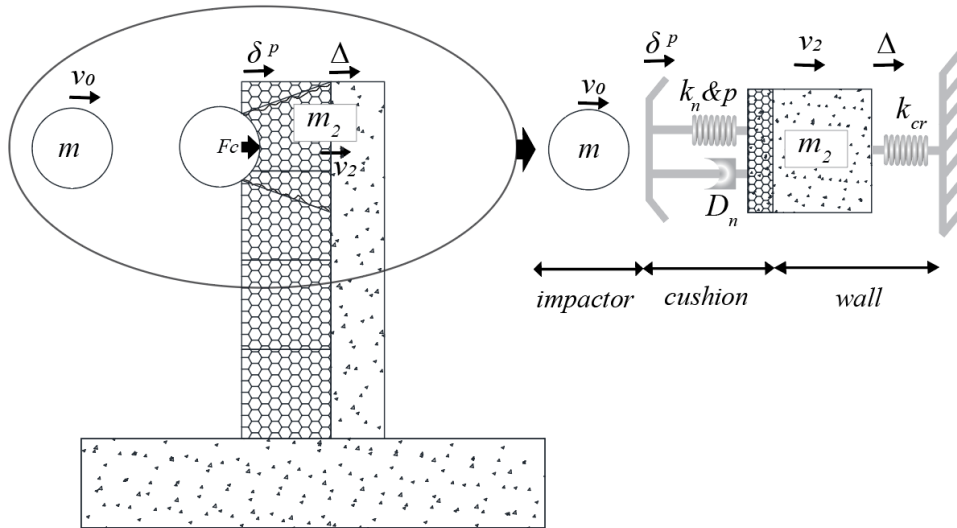
289 In most impact scenarios the amplitude of the contact force can be an order of magnitude higher
290 than the quasi-static force as illustrated in Refs. [20] and [21].

291 However, when the barrier is protected by a layer of cushioning material the impact action is
292 transformed into an impulse. The amplitude and duration of the impulse depend on the design of
293 the cushion. The transformed impulse becomes a forcing function which is then transmitted to
294 the barrier. This forcing function has a certain natural period which may be close to the natural
295 period of the stem wall. If these two natural periods happen to be similar significant dynamic
296 amplification of the target structure can occur. This can result in a potential scenario where the
297 intensity of the contact force can be equal to, or slightly lower than, that of the quasi-static force.
298 This change is beneficial and is to do with the duration of contact being prolonged significantly.
299 Therefore, numerical calculations based on momentum conservation similar to what is given in
300 Ref [22] cannot be applied for determining the deflection demand of a barrier which is protected
301 by a layer of cushioning material.

302 **4.1 Two-degrees-of-freedom (2DOF) system**

303 The Modified Swiss Equation (Eq. (5)) that has been introduced, and validated, provides
304 predictions of the peak contact force which is transmitted to the surface of a RC wall which is
305 protected by gabions. The next step is to model the time-history of the contact force which is
306 referred herein as the forcing function. Modelling the impact generated forcing function is
307 accomplished by the use of a spring connected lumped mass model which is made up of two
308 lumped masses. Hence, the model is described as a two-degrees-of-freedom (2DOF) system as
309 depicted in Fig. 6. Excel spreadsheet calculations with standard row and column operations are
310 used in the 2DOF calculation process which can be used conveniently by practising engineers in
311 the design office environment [23]. The amount of force that is taken up by the frontal spring of
312 the 2DOF system represents the impact generated contact force (F_c). The two lumped masses
313 are: (i) the lumped mass representing the impactor which is connected to the frontal spring (m)

314 and (ii) the lumped mass representing a portion of the gabion cushion and the effective mass of
 315 the RC cantilevered wall (m_2) which is connected to its support through the rear spring. The
 316 layer of granular material is considered to possess response behaviour likened that of
 317 viscoelastic plastic indentation behaviour as reported in Refs. [24, 25]. Thus, the frontal spring
 318 is taken to possess hysteretic properties as defined by the Hunt and Crossley model whereas the
 319 rear spring is modelled to behave in a linear elastic manner assuming that the RC stem wall
 320 responds within the limit of yield. It is important to note that the Hunt and Crosley model has
 321 only been used for modelling hard impact. This paper explores the applicability of the same
 322 contact force model for simulating soft impact and is a novel feature of this article.



323

324

Fig. 6 2DOF simplification

325 **4.2 Combined mass of the wall and cushion (m_2)**

326 The second lumped mass (m_2) which is supported by the rear spring represents a portion of
 327 cushioning material in the vicinity of the point of contact in combination with the participating
 328 mass of the cantilevered wall. Selection of values for lumped mass (m_2) is usually
 329 straightforward for a solid target. However, in this case, both the gabion cushion (m_{gabion}) and
 330 the cantilevered wall (m_{wall}) may be considered to be part of the “target”. Thus, the combined
 331 mass participating in the response to the impact can be represented by Eq. (6). The gabion

332 cushion and the RC stem wall are considered as separate structures responding to the impact
333 action.

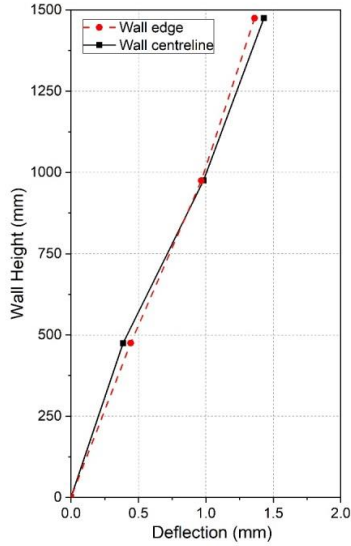
$$m_2 = m_{wall} + m_{gabion} \quad (6)$$

334 The portion of the cushion material that is activated by the impact in the immediate
335 surroundings of the point of contact has been found to be funnel in shape [9, 14, 26]. For
336 crushed rocks, the angle of the funnel may be taken as 30° as per recommendations reported in
337 Refs.[9, 14]. According to Stoffel [15], this value can vary from 33° to 47°. However, what has
338 been reported in the literature is only limited to horizontally layered crushed rock particles. This
339 angle could be different for cushion materials that are confined in a gabion cage. Experiments
340 have been conducted to determine the amount of contributory mass of the gabion cushion by the
341 author as given in Ref [13]. It was identified that the funnel of the activated mass of particles in
342 a layer of gabions had an angle in the range: 20° - 37°, and the angle would not vary
343 significantly with changes in the fill material type. The smaller the angle the lesser the
344 contributory mass of the gabion cushion in developing inertial resistance. Hence, 20° is
345 recommended to be taken as the design funnel angle of the gabion cushion to result in a
346 conservative prediction. The activated or participating mass of the gabion cushion (m_{gabion}) can
347 be calculated using the generalised expression of Eq. (7) which is based on the volume of a
348 funnel where r is the radius of an equivalent sphere of the impactor (radius of the contact) and
349 r_1 is the radius of the force transmitted area (Fig. 6).

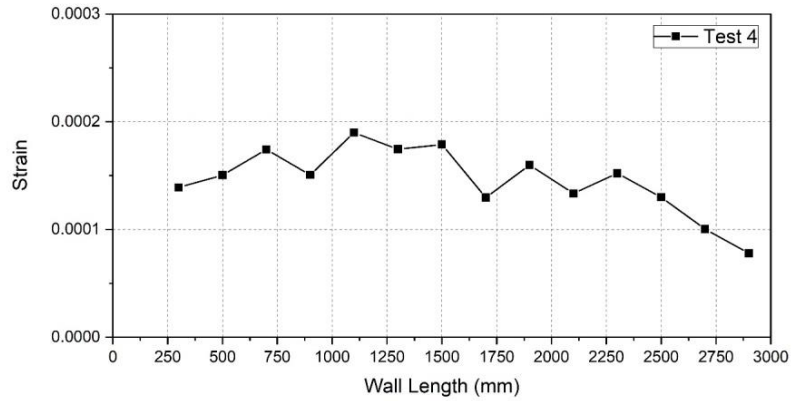
$$m_{gabion} = \frac{1}{3}\pi(r_1^2 + r_1r + r^2)e\rho \quad (7)$$

350 The effective length of the wall undergoing flexural action could be taken as twice the height of
351 the stem wall based on a distribution angle of 45° [22]. This assumed distribution has been
352 confirmed by observing consistent readings from laser sensors and strain gauges that were
353 placed at different locations along the length of the wall. Deflection (up the wall height at the
354 edge and centreline) and the amount of tensile strain experienced by the reinforcing bars close to

355 the base is illustrated in Fig. 7 (a) and Fig. 7 (b) respectively (Test 4 is used as an example to
 356 justify this). Further validations of the cantilevered wall assumption are given in Ref [27] based
 357 on numerical simulations by LS-DYNA. Therefore, the value of m_{wall} may be taken as a
 358 quarter of the mass of the cantilever wall (650kg - lumped mass of the cantilever wall) based on
 359 established structural dynamics principles [28-30].



(a) Deflection of the wall



(b) Tensile strain of longitudinal reinforcement

360 **Fig. 7 Experimentally measured flexural response of the wall: Test 4**

361 **4.3 Rear spring (k_{cr})**

362 Stiffness of the RC stem wall as derived from the principles of structural dynamics takes the
 363 same form as static stiffness (for a cantilevered wall), as shown by Eq. (8) [22].

$$k_{cr} = \frac{3EI_{cr}}{h^3} \quad (8)$$

364 Given the wall height (h), the only parameter to be input into Eq. (8) is the flexural rigidity of
 365 the wall section (EI_{cr}) where subscript cr denotes cracked concrete and this parameter depends
 366 on the location of reinforcing bars (see Figure 1 (b) for details). Moment-curvature analyses
 367 have been undertaken using program Response 2000 [31] for calculating the value of EI_{cr} of
 368 the tested wall section. Apart from the moment curvature analysis, a simplified method of

369 calculation employing Eqs. (9) to (11) can also be used for calculating the value of EI_{cr} . There
370 are two underlying assumptions: 1) the tensile longitudinal reinforcement of the stem wall must
371 be responding within the limit of yield and 2) there is no occurrence of any signs of brittle
372 failure on the wall. Eq. (9) is based on the well-established Whitney stress block model (as
373 introduced in Ref. [32]) whereas Eq. (10) was derived from Priestley, Calvi and Kowalsky [33]
374 based on extensive moment-curvature analyses on a lightly (axially) loaded structural elements
375 consistent with the conditions of the cantilevered wall. The estimated value of EI_{cr} is translated
376 to $k_{cr} = 14379 \text{ kN/m}$ which represents the flexural stiffness of the RC stem wall in cracked
377 conditions.

$$M_y = \phi M_u = 0.8 A_{st} f_y d \left(1 - 0.6 \frac{A_{st} f_y}{B d f'_c} \right) \quad (9)$$

$$\phi_y = \frac{1.7 \varepsilon_{sy}}{D} \quad (10)$$

$$EI_{cr} = \frac{M_y}{\phi_y} \quad (11)$$

378 **4.4 Frontal spring**

379 Parameters characterising the frontal spring (as per Hunt & Crossley Model) are namely the
380 spring stiffness k_n , exponent p and damping coefficient D_n as shown by Eq. (12). Different
381 expressions for determining the value of D_n can be found in the literature [34-38] Eq. (13)
382 which was derived recently presents D_n as function of k_n and p [39-41]. $\dot{\delta}_0 = v_0$ may be
383 assumed for input into Eq. (13) given that the barrier is initially at rest.

$$F_c = k_n \delta^p + D_n \delta^p \dot{\delta} \quad (12)$$

$$D_n = (0.2p + 1.3) \left(\frac{1 - \text{COR}}{\text{COR}} \right) \frac{k_n}{\dot{\delta}_0} \quad (13)$$

384 The expression of Eq. (14) for determining the value of the COR parameter is based on
385 Newton's impact hypothesis. More details of this derivation are given in Ref [42].

$$\text{COR} = \frac{v_1 + v_2}{v_0} \quad (14)$$

386 where v_1 is the velocity of the boulder on rebound (in the opposite direction of the impact), and
 387 v_2 is the velocity of the idealised lumped mass representing the responding cantilevered wall
 388 and the loaded portion of the gabion (Fig (6)).

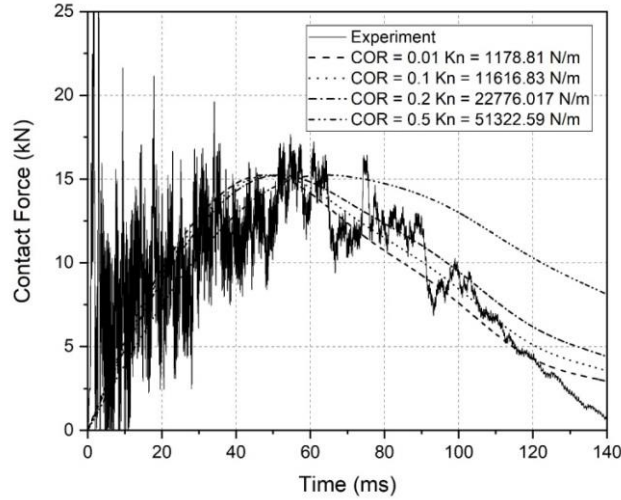
389 Solution to Eq. (12) for the value of maximum contact force (F_{cmax}) is presented in the form of
 390 a closed form expression as shown by Eq. (15) which was first introduced in Ref [20]. Details of
 391 the derivation can be found in Appendix B. Parameter λ_2 which appears in Eq. (15) is
 392 introduced herein to denote the ratio of the combined target mass (i.e. m_2 as defined by Eq. (6))
 393 and the mass of the impactor (i.e. m_2/m).

$$F_{cmax} = k_n \left[1 + (0.2p + 1.3) \left(\frac{1 - \text{COR}}{\text{COR}} \right) \left(\frac{-b + \sqrt{b^2 + 4c}}{2} \right) \right] \times \left(\frac{p + 1}{2k_n} \left(\frac{\lambda_2}{1 + \lambda_2} \right) m v_0^2 \text{COR} \right)^{\frac{p}{p+1}} \times \left[1 - \left(\frac{-b + \sqrt{b^2 + 4c}}{2} \right)^2 \right]^{\frac{p}{2}} \quad (15)$$

394 where $b = \frac{p \times \text{COR}}{(1+p)(0.2p+1.3)(1-\text{COR})}$ and $c = \frac{1}{p+1}$

395 The value of COR can be determined from experimental measurements of the velocity of
 396 motion of the impacted objects. Alternatively, a method for finding the value of COR in an
 397 elastoplastic contact has been proposed by Thornton [43]. Neither method is suited to situations
 398 where the response time of the cantilevered wall of the barrier (wall placed behind the cushion)
 399 is too short in comparison with the much prolonged compression of the cushioning material. It
 400 was observed from video capture of the cushioned impact that the impactor became attached to,
 401 or embedded into, the gabion cushion. Thus, in theory, $\text{COR} = 0$ may be assumed. However, the
 402 value of D_n as defined by Eq. (13) would be mathematically undefinable if $\text{COR} = 0$. To
 403 circumvent this issue, a very small value of COR ($= 0.01$) has been taken. Fig. 8 compares
 404 contact force occurring on impact as recorded by the accelerometer in Test 4 with predictions

405 from the 2DOF model assuming different values of COR . It was found from a sensitivity
 406 analysis that varying the value of COR in the range 0.01 - 0.2 would result in insignificant
 407 changes to the simulated behaviour of the target.



408

409

Fig. 8 Sensitivity analysis to changes in the value of COR: Test 4

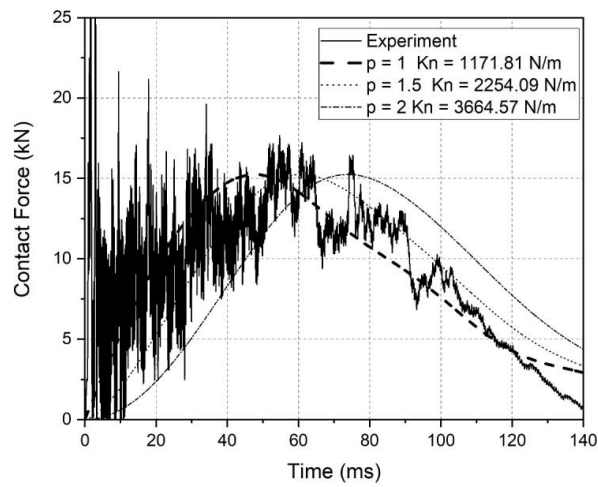
410 The deformation behaviour of the cushion layer can be modelled assuming viscoelastic plastic
 411 behaviour when subject to an impact action [24, 25, 44]. To simplify the computations linear
 412 viscoelastic behaviour (i.e. $p = 1$) may be assumed whereas the assumption of non-linearity on
 413 contact (i.e. $p > 1$) would delay the occurrence of the rise of the contact force. No such “delay”
 414 phenomenon was observed from the impact tests. Three types of forcing functions are shown for
 415 comparison in Fig. 9 based on taking $COR = 0.01$. It was found from sensitivity analyses in
 416 which the value of p was varied within the range: $1 < p < 2$ that the simulated response
 417 behaviour matched best with experimental recorded behaviour when $p = 1$ was assumed. The
 418 contact force model of Eq. (12) is accordingly simplified into Eq. (16).

$$F_c = k_l \delta + D_l \delta \dot{\delta} \quad (16)$$

419 where k_l is the linear spring stiffness and D_l is the damping coefficient ($k_n = k_l$ and $D_n = D_l$
 420 when $p = 1$). The value of parameter D_l may be found using Eq. (17) which is a special case
 421 with $p (= 1)$ and $COR (= 0.01)$ based on the generalised relationship of Eq. (13).

$$D_l = 148.5 \frac{k_l}{\dot{\delta}_0} \quad (17)$$

422 In Fig. 9, the forcing function that has been simulated as per the special case of Hunt & Crossley
 423 model based on Eq. (16) and Eq. (17) is shown by a thicker line ($p = 1$). The comparison
 424 between the predicted and recorded forcing functions only shows order of magnitude agreement
 425 (as the high level of noise that has been recorded is not featured in the predictive model). Note
 426 that the results presented here have already been filtered using a Butterworth filter to remove
 427 high-frequency noise. The noise in experimental results is to do with the impactor touching with
 428 the rock particles and causing them to slip.



429

Fig. 9 Sensitivity to change in the value of p : Test 4

430

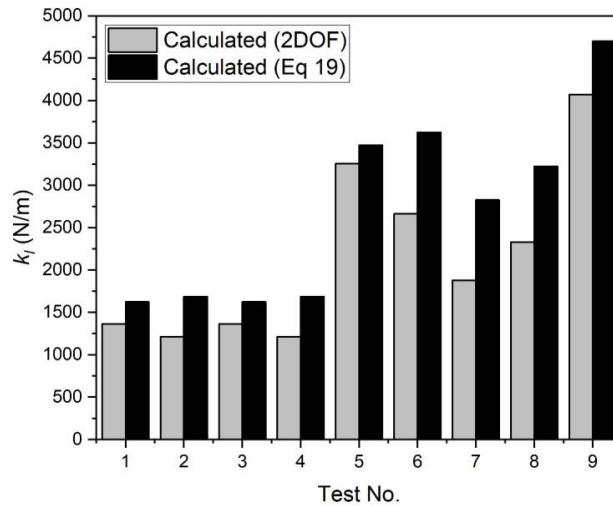
431 Take $p = 1$ and $COR = 0.01$ as justified earlier. Notation is changed from k_n to k_l . Eq. (15) is
 432 then simplified into Eq. (18).

$$F_{cmax} = k_l \times \left(\frac{1}{k_l} \left(\frac{\lambda_2}{1 + \lambda_2} \right) m v_0^2 \right)^{\frac{1}{2}} \times 7.5 \quad (18)$$

433 Eq. (18) can be rearranged into Eq. (19) in which k_l is expressed as function of the peak contact
 434 force F_{cmax} along with impact parameters: m , v_0 and λ_2 . The factor appearing in the
 435 denominator was found to be between 50-60. A rounded-off value of 50 is taken as this would
 436 result in a slightly more conservative estimates of the stiffness, and hence contact force.

$$k_l = \frac{F_{cmax}^2}{50 m v_0^2} \times \left(\frac{1 + \lambda_2}{\lambda_2} \right) \quad (19)$$

437 In summary, the value of k_l can be found using Eq. (19) once the peak contact force (F_{cmax}) is
 438 known. The value of F_{cmax} can be estimated using the Modified Swiss Equation of Eq. (5)
 439 which in turn requires knowledge of the modulus of subgrade reaction (M_E). The method of
 440 obtaining M_E by static testing has been presented in section 2. The comparison between the
 441 numerically simulated and calculated values of k_l (by Eq. (19)) is presented in the form of a bar
 442 chart as shown in Fig. 10. It is shown that predictions for the value of k_l as obtained from the
 443 use of Eq. (19) are only slightly higher, and hence more conservative, than results inferred from
 444 numerical simulations of the 2DOF system model.

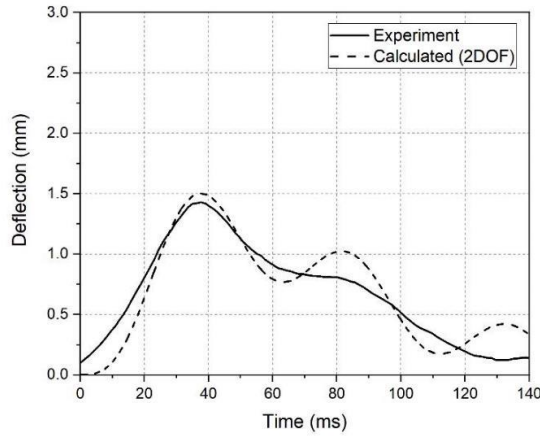


445
 446 **Fig. 10 Comparison of k_l calculated using 2DOF model with predictions from Eq. (19)**

447 **4.5 The deflection of the RC stem wall**

448 Having determined the value of k_l , p and COR (hence D_l) the deflection time-histories of the
 449 responding target can be simulated (using the 2DOF system model) for comparison with time-
 450 histories recorded from the impact experiments. The proposed analytical model has been
 451 validated further by comparison of the experimentally recorded deflection of the RC wall with
 452 model predictions (as indicated by the movement of the rear lumped mass in the 2DOF model).
 453 The deflection of the RC stem wall was monitored by laser sensors which were mounted up the
 454 height of the wall at the centreline. In Fig. 11, reasonable agreement between the simulated and
 455 the recorded time-history deflection data from Test 4 is demonstrated.

456 In Fig. 12, maximum deflection values of the wall as inferred from the recorded time history
 457 data are shown alongside analytical predictions from the 2DOF system model for all the
 458 cushioned impact tests that have been conducted. The ability of the analytical model to give
 459 reasonably accurate predictions of the deflection demand of the RC stem wall is well
 460 demonstrated. Deflection demand of the wall without a protective cushion layer (control
 461 experiment) is also presented in Fig. 12 for comparison purposes. The presented results
 462 demonstrate that the maximum deflection of the wall with a protective cushion layer is much
 463 lower than the control experiment of the bare wall. The amount of reduction in deflection was
 464 more than 70% in most cases.

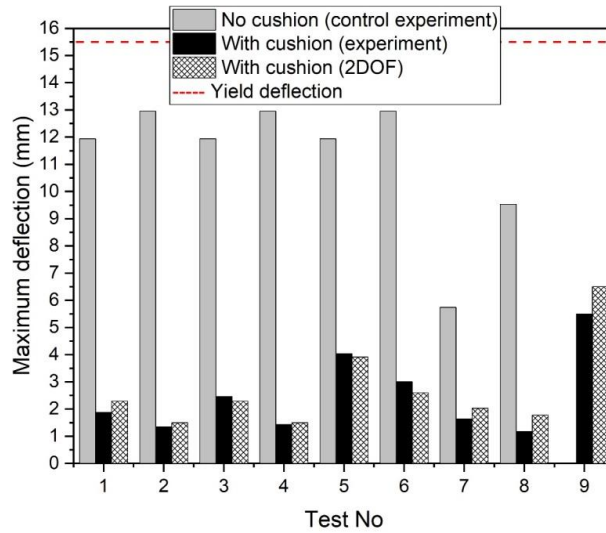


465
 466 **Fig. 11 Comparison of time-histories of deflection at top middle of the wall for Test 4**

467 Yield deflection is also presented in the same figure which was calculated based on the wall
 468 properties prior to the experiment. Given that the value of the yield curvature (ϕ_y) of the
 469 cantilevered wall has been calculated using Eq. (10), being 0.021 rad/m, the value of the yield
 470 deflection (Δ_y) can be estimated using Eq. (20) and Eq. (21) as established on Ref [45], being
 471 15.5 mm. In this, h_i represents the impact height and not to be confused with the wall height h
 472 (h_i is slightly lower than the wall height h).

$$\Delta_{yi} = \frac{\phi_y h_i^2}{3} \quad (20)$$

$$\Delta_y = \Delta_{yi} \left(\frac{3h - h_i}{2h_i} \right) \quad (21)$$



473
 474 **Fig. 12 Comparison of experiment and prediction of 2DOF model for maximum deflection at top**
 475 **middle of wall**

476 **5 A Simplified Analytical Procedure**

477 A displacement-based model was developed by Lam, Yong, Lam, Kwan, Perera, Disfani and
 478 Gad [46] to predict the performance behaviour of reinforced concrete barrier when subjected to
 479 the impact of a boulder on the cantilevered wall causing it to deflect and bend. Detailed
 480 descriptions and derivations of the model by the authors and co-workers have been reported in
 481 the literature [47-50].

482 The analytical model of Eq.(22) for estimating the displacement demand of an impact has been
 483 derived, and experimentally validated, for conditions where the target is responding within the
 484 elastic limit [46]. Input to the equation is the impactor mass (m), stiffness of the target
 485 responding within the elastic limit (k), generalised mass of the target (λm), and coefficient of
 486 restitution (COR). For specific conditions where the impactor does not rebound (i.e. $COR = 0$)
 487 but is instead embedded into the surface of the target Eq.(22) is reduced to Eq.(23) which was
 488 first presented in Ref. [50].

489 If the target is a lightly loaded RC element such as a RC stem wall which is susceptible to
 490 cracking on impact “ k ” is replaced by “ k_{cr} ” where subscript “cr” denotes cracked concrete. In

491 the case of an impact that is cushioned by a layer of gabion Eq. (23) is modified further into Eq.
 492 (24) in which the γ factor is introduced to allow for the mitigation effects of the impact action
 493 resulted from the gabion cushion delaying the transmission of momentum to the barrier. The
 494 second term on the right-hand side of Eq.(24) which is similar in form to the right hand side of
 495 Eq.(23) can be used to estimate the deflection demand of an impact scenario where the flying
 496 object becomes attached to (or embedded into) the surface of the target (i.e. COR = 0). This
 497 assumption is supported by observations from all the tests conducted by the investigators when
 498 cushioning was put in place. Note also that the mass ratio of the target ($\lambda = \frac{m_{wall}}{m}$) is denoted
 499 herein as $\lambda_2 = \frac{m_2}{m}$ in Eq. (24) to facilitate the effect of cushioning as a combined target mass.

$$\Delta \sim \frac{mv_0}{\sqrt{mk}} \sqrt{\lambda \left(\frac{1 + COR}{1 + \lambda} \right)^2} \quad \text{as derived in Refs. [32] \& [56]} \quad (22)$$

500 An important distinction between Eq. (22) and (23) rests with the condition of impact and
 501 rebound. Eq. (22) deals with the impactor rebounding from the target after making a one-off
 502 contact. In contrasts, Eq. (23) deals with the impactor becoming attached to the target forming a
 503 combined mass. As the latter condition is consistent with that of a cushioned impact, Eq. (23) is
 504 modified into Eq. (24) to incorporate the γ multiplier to take into account the further reduction
 505 of the displacement demand resulted from cushioning. The alternative derivation by Refs. [38]
 506 and [40] suggests that the maximum deflection is proportional to the impactor momentum at
 507 impact and that rebound is negligible.

$$\Delta \sim \frac{mv_0}{\sqrt{mk(1 + \lambda)}} \quad \text{as derived in Ref. [40]} \quad (23)$$

$$\Delta \sim \gamma \frac{mv_0}{\sqrt{mk_{cr}(1 + \lambda)}} \quad \text{as derived in Ref. [38]} \quad (24)$$

508 One of the main functionalities of the cushion is to delay the transfer of momentum thereby
 509 resulting in a further reduction in the deflection demand of the impact. The γ factor (the first

510 term in Eq. (24)) is to represent this further reduction which is resulted from the delay and is
 511 shown to be correlated with the time taken for the contact force to rise to its peak (i.e. “*rise*
 512 *time*”) in the forcing function. The time taken by the target to deflect to the full extent in
 513 response to the impact is the “*response time*”. The ratio of *rise time: response time* can be
 514 represented by the natural period ratios (T_m/T_{m_2}) of the two lumped masses in the two-degree-
 515 of-freedom (2DOF) system representation.

516 The value of the γ factor can be found by applying the following calculation:

- 517 1. Calculation for determining the value of T_m/T_{m_2} using Eq. (25) and
- 518 2. Calculation for determining the value of γ as function of T_m/T_{m_2} and λ_2 using the chart
 519 of Fig. 13

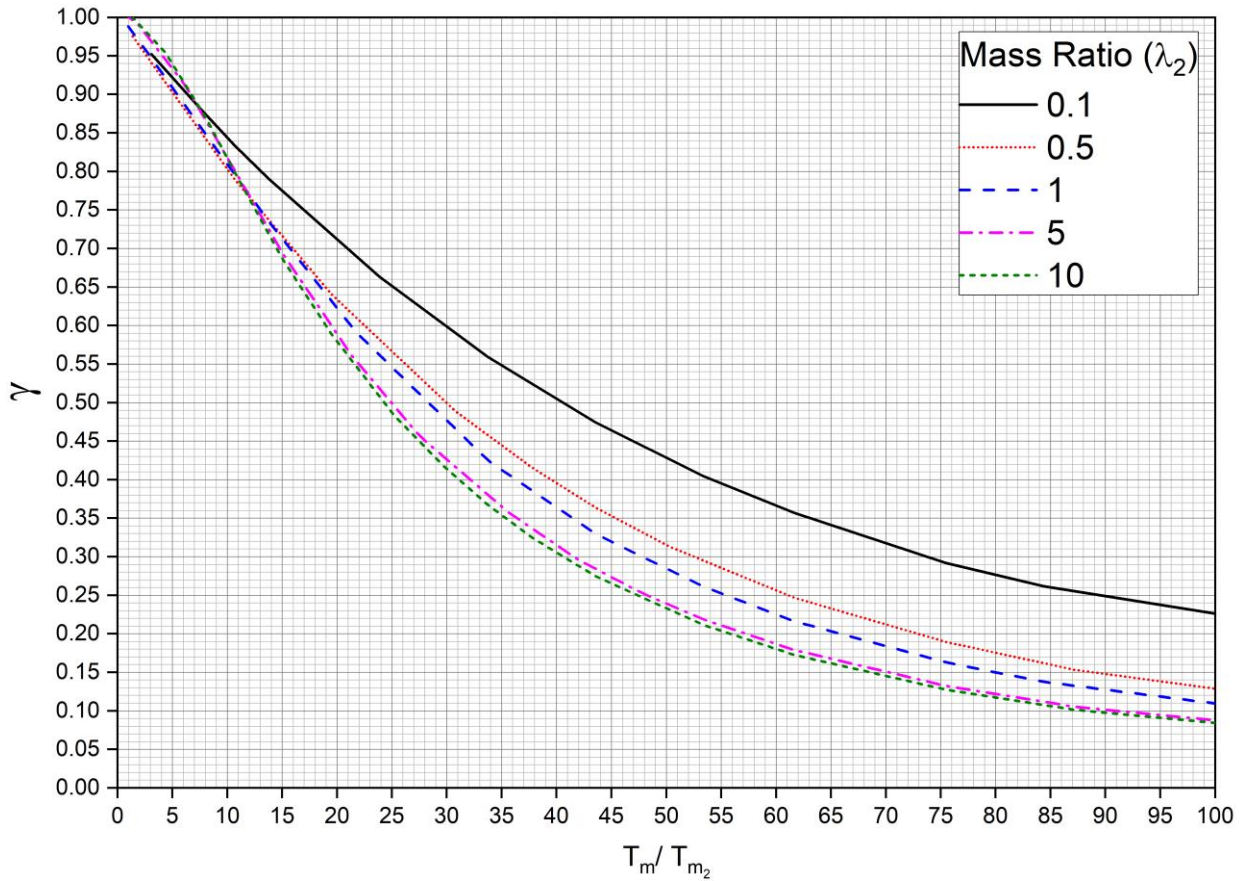
$$\frac{T_m}{T_{m_2}} = 2\pi \sqrt{\frac{mk_{cr}}{m_2k_l}} \quad (25)$$

520 where m , m_2 , k_{cr} and k_l (or k_n) are as defined in Fig. 6. The chart was developed from a
 521 parametric study which involved analyses making use of the 2DOF system as introduced in
 522 Section 4.

523 The value of k_l which characterises the cushion stiffness must be known beforehand in
 524 determining the value of $\frac{T_m}{T_{m_2}}$ based on use of Eq. (25). Parameter k_l can be found by use of Eq.
 525 (19).

526 In summary, the deflection demand of the impact can be calculated using the closed-form
 527 expression of Eq. (24) along with the design chart of Fig. 13 for identifying the value of γ . The
 528 trends of γ varying with changes in the natural period ratio (T_m/T_{m_2}) and mass ratio (λ_2) as
 529 obtained from parametric studies (based on numerical simulations of the 2DOF model) are well
 530 displayed on this chart.

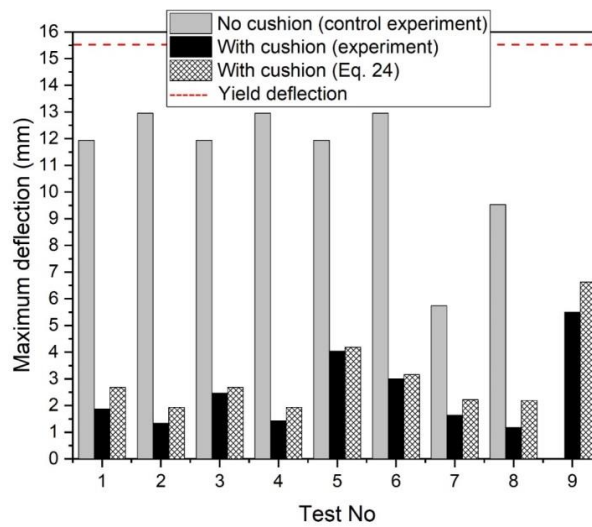
531 The deflection demand of the cushioned impact as obtained from the calculation procedure as
 532 described have been compared with experimentally recorded results in Fig. 14. The deflection
 533 demand recorded from tests is shown to be in good agreement with analytical predictions.



534

535

Fig. 13 Design chart for γ



536

Fig. 14 Comparison of deflection recorded from experiment with predictions from Eq. (24)

538 **6 Conclusion**

539 Pendulum style impact tests have been performed on a full-scale reinforced concrete barrier
540 specimen which had the protection of a layer of gabion (cushion) cover of two different filling
541 materials. Results show that the cushion layer was able to reduce the contact force by more than
542 95% and deflection demand on the RC stem wall by about 70%. The particle properties of the
543 filling material had no significant influence on the amount of reduction whereas a stronger
544 gabion cages (built of larger diameter wire mesh) showed less reduction of the deflection
545 demand of the impact compared to that of more flexible gabion cages. High energy impact
546 (10kJ) test highlights the significance of the mitigation actions of the gabion cushion in terms of
547 reduction in the contact force and the flexural action on the stem wall.

548 An expression for estimating the magnitude of the contact force transmitted across the thickness
549 of the cushion was first presented and experimentally validated. It is shown that the forcing
550 function of impact affecting the cantilevered wall (which was placed behind the cushion) could
551 be simulated reasonably accurately by employing the non-linear viscoelastic model (also known
552 as Hunt and Crossley model) for characterising the hysteretic properties of the frontal spring
553 forming part of the two-degrees-of-freedom (2DOF) spring connected lumped mass system. The
554 2DOF system model so derived has been validated by comparison of the simulated deflection
555 demand with experimental measurements. A closed form expression which is used in
556 conjunction with a design chart has been derived from deflection demand data (that was
557 generated from parametric studies employing the 2DOF system model) to facilitate uptake in
558 design practices. A worked example is given at the Appendix A for ease reference of the
559 proposed methodology.

560 This article deals with quantifying the mitigation actions of the gabion materials on the
561 deflection demand on the stemwall of a rockfall barrier in an impact scenario. This is an original
562 contribution as no similar initiatives has been reported in the literature. The provision of a hand
563 calculation procedure involving the use of a design chart is an added original feature to the

564 presented design methodology which is limited to conditions where the stemwall responds
565 within the limit of yield and there is no sign of occurrence of brittle fracture. Another limitation
566 of the procedure is that the wall is not too flexible that it becomes necessary to take into account
567 effects of the higher modes.

568 There are scopes for further investigations for modelling the deflection demand on the cushion
569 protected stem wall taking into account the effects of multiple strikes at the same position on the
570 cushion and further developing the methodology by testing wall specimens to respond beyond
571 the yield limit.

572 7 References

- 573 [1] R. Chikatamarla, J. Laue, S. Springman, Rockfall impact on protection galleries, in: Second
574 International Conference of Structural Engineering Mechanics and Computations, Balkema,
575 Rotterdam, Cape Town, South Africa, 2004, pp. 1139-1144.
- 576 [2] A. Heymann, M. Collombet, S. Lambert, P. Gotteland, Use of external testing methods to
577 assess damage on rockfall protection structures, in: Applied Mechanics and Materials, Trans
578 Tech Publ, 2011, pp. 704-709.
- 579 [3] S. Lambert, A. Heymann, P. Gotteland, F. Nicot, Real-scale investigation of the kinematic
580 response of a rockfall protection embankment, Natural Hazards and Earth System Sciences, 14
581 (2014) p. 1269-p. 1281.
- 582 [4] C. Ng, C.E. Choi, Y. Su, J. Kwan, C. Lam, Large-Scale Successive Boulder Impacts on a
583 Rigid Barrier Shielded by Gabions, Canadian Geotechnical Journal, (2016).
- 584 [5] F. Calvetti, C. Di Prisco, M. Vecchiotti, Experimental and numerical study of rock-fall
585 impacts on granular soils, Rivista Italiana di Geotecnica, 4 (2005) 95-109.
- 586 [6] N. Kishi, H. Konno, K. Ikeda, K. Matsuoka, Prototype impact tests on ultimate impact
587 resistance of PC rock-sheds, International Journal of Impact Engineering, 27 (2002) 969-985.
- 588 [7] V. Labiouse, F. Descoeurdes, S. Montani, C. Schmidhalter, Experimental study of rock
589 blocks falling down on a reinforced concrete slab covered by absorbing cushions, Revue
590 française de géotechnique, 69 (1994) 41-61.
- 591 [8] K. Schellenberg, A. Volkwein, A. Roth, T. Vogel, Rockfall–Falling weight tests on galleries
592 with special cushion layers, in: Proceedings, 3rd international conference on protection of
593 structures against hazards, September, 2006, pp. 28-29.
- 594 [9] F. Calvetti, Distinct Element evaluation of the rock-fall design load for shelters, Rivista
595 Italiana di geotecnica, 3 (1998) 63-83.
- 596 [10] H. Yoshida, Recent experimental studies on rockfall control in Japan, in: Joint Japan-Swiss
597 Scientific Seminar on Impact Load by Rock Falls and Design of Protection Structures,
598 Kanazawa, Japan, 1999.
- 599 [11] R. Agostini, Flexible gabion structures in earth retaining works, Officine Maccaferri, 1987.
- 600 [12] H. Hertz, Über die Berührung fester elastischer Körper. On the contact of elastic solids,
601 Reine und angewandte Mathematik. London:(Instruction anglaise dans Miscellaneous papers by
602 H. Hertz) Eds Jones et Schaott, in, Macmillan, 1896.

603 [13] J.S. Perera, N. Lam, M.M. Disfani, E. Gad, Impact response behaviour of gabion cells filled
604 with different cushion, in: ACMSM25, Brisbane, 2018.

605 [14] ASTRA, Einwirkungen infolge Steinschlags auf Schutzgalerien, Richtlinie, Bundesamt für
606 Strassen, Baudirektion SBB, Eidgenössische Drucksachen- und Materialzentrale, Bern., (2008).

607 [15] S.M. Stoffel, Sollicitation dynamique de la couverture des galeries de protection lors de
608 chutes de blocs, in, Verlag nicht ermittelbar, 1998.

609 [16] K. Bucher, Dynamische Berechnung von Steinschlageinwirkungen, in: Proceedings,
610 Schweizerische Gesellschaft für Boden und Felsmechanik, Conference Paper Montreux, 1997.

611 [17] S. Degago, R. Ebeltoft, S. Nordal, Effect of rock fall geometries impacting soil cushion: a
612 numerical procedure, in: proceedings of the 12th International Conference of International
613 Association for Computer Methods and Advances in Geomechanics (IACMAG), Goa, India,
614 2008, pp. 1-6.

615 [18] V. Labiouse, F. Descoedres, S. Montani, Experimental study of rock sheds impacted by
616 rock blocks, *Structural Engineering International*, 6 (1996) 171-176.

617 [19] D.-G. Lin, Y. Lin, F. Yu, Deformation analyses of gabion structures, *INTERPRAEVENT*
618 2010, (2010) 512-526.

619 [20] J. Sun, Lam, N., Zhang, L., Ruan, D. and Gad, E., Contact forces generated by hailstone
620 impact, *International Journal of Impact Engineering*, 84 (2015) 145-158.

621 [21] S. Perera, Lam, N., Pathirana, M., Zhang, L., Ruan, D. and Gad, E., Deterministic solutions
622 for contact force generated by impact of windborne debris, *International Journal of Impact*
623 *Engineering*, 91 (2016) 126-141.

624 [22] A.C. Yong, N.T. Lam, S.J. Menegon, E.F. Gad, Experimental and Analytical Assessment
625 of Flexural Behavior of Cantilevered RC Walls Subjected to Impact Actions, *Journal of*
626 *Structural Engineering*, 146 (2020) 04020034.

627 [23] N. Lam, H. Tsang, E. Gad, Simulations of response to low velocity impact by spreadsheet,
628 *International Journal of Structural Stability and Dynamics*, 10 (2010) 483-499.

629 [24] C. Di Prisco, M. Vecchiotti, A rheological model for the description of boulder impacts on
630 granular strata, *GEOTECHNIQUE-LONDON-*, 56 (2006) 469.

631 [25] R. Chikatamarla, Optimisation of cushion materials for rockfall protection galleries, PhD
632 Dissertation, vdf Hochschulverlag AG, 2007.

633 [26] Japan Road Association, Manual for anti-impact structures against falling rocks (in
634 Japanese). (1983).

635 [27] A.C.Y. Yong, Impact-resistance of Reinforced Concrete Structures, in, 2019.

636 [28] J.S.P. Pethati Mudiyansele Don, Rigid Barrier with a Gabion Cushion Subjected to
637 Boulder Impact, in, 2019.

638 [29] J. Sun, N. Lam, L. Zhang, D. Ruan, E. Gad, Computer Simulation of Contact Forces
639 Generated by Impact, in: *International Journal of Structural Stability and Dynamics*, 2016.

640 [30] A.C.Y. Yong, Closed-form Expressions for Improved Impact Resistant Design of
641 Reinforced Concrete Beams, Structures, (2021).

642 [31] E.C. Bentz, Sectional analysis of reinforced concrete members, University of Toronto
643 Toronto, 2000.

644 [32] R. Park, T. Paulay, Reinforced concrete structures, John Wiley & Sons, 1975.

645 [33] M.J.N. Priestley, G.M. Calvi, M.J. Kowalsky, Displacement-Based Seismic Design of
646 Structures, IUSS Press, Pavia, Italy, 2007.

647 [34] R.G. Herbert, D.C. McWhannell, Shape and Frequency Composition of Pulses From an
648 Impact Pair, *Journal of Manufacturing Science and Engineering*, 99 (1977) 513-518.

649 [35] T.W. Lee, A.C. Wang, On The Dynamics of Intermittent-Motion Mechanisms. Part 1:
650 Dynamic Model and Response, *J. Mech. Des.*, 105 (1983) 534-540.

651 [36] H.M. Lankarani, P.E. Nikraves, A contact force model with hysteresis damping for impact
652 analysis of multibody systems, *J. Mech. Des.*, 112 (1990) 369-376.

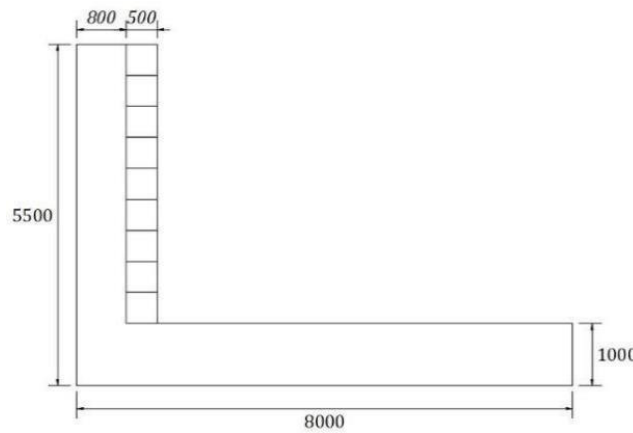
- 653 [37] Y. Gonthier, J. McPhee, C. Lange, J.C. Piedboeuf, A regularized contact model with
654 asymmetric damping and dwell-time dependent friction, *Multibody Syst. Dyn.*, 11 (2004) 209-
655 233.
- 656 [38] P. Flores, M. Machado, M.T. Silva, J.M. Martins, On the continuous contact force models
657 for soft materials in multibody dynamics, *Multibody Syst. Dyn.*, 25 (2011) 357-375.
- 658 [39] J. Sun, N. Lam, L. Zhang, D. Ruan, E. Gad, Contact forces generated by hailstone impact,
659 *International Journal of Impact Engineering*, 84 (2015) 145-158.
- 660 [40] S. Perera, N. Lam, M. Pathirana, L. Zhang, D. Ruan, E. Gad, Deterministic solutions for
661 contact force generated by impact of windborne debris, *Int. J. Impact Eng.*, 91 (2016) 126-141.
- 662 [41] S. Perera, N. Lam, M. Pathirana, L. Zhang, D. Ruan, E. Gad, Use of static tests for
663 predicting damage to cladding panels caused by storm debris, *Journal of Building Engineering*,
664 12 (2017) 109-117.
- 665 [42] A.C. Yong, C. Lam, N.T. Lam, J.S. Perera, J.S. Kwan, Analytical solution for estimating
666 sliding displacement of rigid barriers subjected to boulder impact, *Journal of Engineering*
667 *Mechanics*, 145 (2019) 04019006.
- 668 [43] C. Thornton, Coefficient of restitution for collinear collisions of elastic-perfectly plastic
669 spheres, *Journal of Applied Mechanics*, 64 (1997) 383-386.
- 670 [44] C. di Prisco, M. Vecchiotti, Design charts for evaluating impact forces on dissipative
671 granular soil cushions, *Journal of geotechnical and geoenvironmental engineering*, 136 (2010)
672 1529-1541.
- 673 [45] A.C. Yong, N.T. Lam, S.J. Menegon, E.F. Gad, Cantilevered RC Wall Subjected to
674 Combined Static and Impact Actions, *International Journal of Impact Engineering*, (2020)
675 103596.
- 676 [46] N.T. Lam, A.C. Yong, C. Lam, J.S. Kwan, J.S. Perera, M.M. Disfani, E. Gad,
677 Displacement-based approach for the assessment of overturning stability of rectangular rigid
678 barriers subjected to point impact, *Journal of Engineering Mechanics*, 144 (2017) 04017161.
- 679 [47] N.T.K. Lam, A.C.Y. Yong, C. Lam, J.S.H. Kwan, J.S. Perera, M.M. Disfani, E. Gad,
680 Displacement-based approach for the assessment of overturning stability of rectangular rigid
681 barriers subjected to point impact, *Journal of Engineering Mechanics*, 144 (2018).
- 682 [48] N. Lam, E. Gad, The estimation of impact forces based on first principles, in: *Australasian*
683 *Structural Engineering Conference: ASEC 2016*, Engineers Australia, 2016, pp. 350.
- 684 [49] Y. Yang, N.T.K. Lam, L. Zhang, Evaluation of simplified methods of estimating beam
685 responses to impact, *International Journal of Structural Stability and Dynamics*, 12 (2012)
686 1250016-1250011-1250016-1250024.
- 687 [50] M. Ali, J. Sun, N. Lam, L. Zhang, E. Gad, Simple hand calculation method for estimating
688 deflection generated by the low velocity impact of a solid object, *Australian Journal of*
689 *Structural Engineering*, 15 (2014) 243-259.
- 690 [51] S. Perera, Modelling impact actions of flying and falling objects, in, 2017.

691

692

693 **Appendix A - worked Example for Illustration of the Simplified Procedure**

694 The rigid barrier considered in this worked example is to withstand a rockfall event of 1.5 m
 695 diameter boulder impacting at 7 ms⁻¹ velocity. The 10 m long rigid barrier is protected by 0.5 m
 696 thick gabions cushion layer which has a bulk density of 1500 kg/m³ (Fig. A1). It is designed
 697 with 40 mm reinforcement at 200 mm spacing. Other parameters used for the design are as
 698 follows: $f'_c = 32$ MPa, $f_y = 500$ MPa, $E = 200$ GPa, $M_E = 3000$ kPa (assuming the use of strong
 699 cages as cushion), $\phi_k = 40^\circ$. Calculation is considered on per metre length of wall basis.



700

701

Fig. A1 Dimensions of rigid barrier

702
$$A_{st} = \frac{1000}{200} \times \pi \left(\frac{40}{2} \right)^2 = 6283.2 \text{ mm}^2/\text{m}$$

703
$$M_y = 0.8 A_{st} f_y d \left(1 - 0.6 \frac{A_{st} f_y}{B d f'_c} \right)$$

704
$$= 0.8 \times 6283.2 \times 500 \times 700 \times \left(1 - 0.6 \times \frac{6283.2 \times 500}{1000 \times 700 \times 32} \right) \times 10^{-6} = 1611 \text{ kNm/m}$$

705
$$L_{eff} = 2(h) = 2 \times (5.5 - 1) = 9 \text{ m}$$

706
$$M_y = 1611 \times 9 = 14501 \text{ kNm}$$

707
$$\varepsilon_{sy} = \frac{f_y}{E} = \frac{500}{200000} = 0.0025; \phi_y = \frac{1.7 \varepsilon_{sy}}{D} = \frac{1.7(0.0025)}{0.8} = 0.0053125 \text{ rad/m}$$

708
$$EI_{cr} = \frac{M_y}{\phi_y} = \frac{14501}{0.0053125} = 2729643 \text{ kNm}^2$$

709
$$k_{cr} = \frac{3EI_{cr}}{h^3} = \frac{3(2729643)}{4.5^3} = 89865 \text{ kN/m}$$

$$710 \quad r_1 = r + e \times \tan(20^\circ) = 0.75 + 0.5 \times \tan(20^\circ) = 0.932 \text{ m}$$

$$711 \quad m_{gabion} = \frac{1}{3}\pi(r_1^2 + r_1r + r^2)e\rho_g = \frac{1}{3}\pi(0.932^2 + 0.932 \times 0.75 + 0.75^2)0.5 \times 1500$$

$$712 \quad = 1672 \text{ kg}$$

$$713 \quad m_{wall} = 0.25 \times 0.8 \times 9 \times 4.5 \times 2450 = 19845 \text{ kg}$$

$$714 \quad m_2 = m_{wall} + m_{gabion} = 19845 + 1672 = 21517 \text{ kg}$$

$$715 \quad m = 2650 \times \frac{4}{3}\pi \times \left(\frac{1.5}{2}\right)^3 = 4683 \text{ kg}$$

$$716 \quad \lambda_2 = \frac{m_2}{m} = \frac{21517}{4683} = 4.59$$

$$717 \quad F_{cmax} = 0.65 \times 2.8 \times e^{-0.5} \times r^{0.7} \times M_E^{0.4} \times \tan\phi_k \times \left(\frac{mv_0^2}{2}\right)^{0.6}$$

$$718 \quad = 1.82 \times 0.5^{-0.5} \times 0.75^{0.7} \times 3000^{0.4} \times \tan 40^\circ \times \left(\frac{4.683 \times 7^2}{2}\right)^{0.6} = 747.49 \text{ kN}$$

$$719 \quad k_l = \frac{F_{cmax}^2}{50mv_0^2} \times \left(\frac{1 + \lambda_2}{\lambda_2}\right) = \frac{747.49^2}{50 \times 4683 \times 7^2} \times \left(\frac{1 + 4.59}{4.59}\right) = 59298 \text{ N/m}$$

$$720 \quad T_m = 2\pi \sqrt{\frac{m}{k_l}} = 2\pi \sqrt{\frac{4683}{59298}} = 1.77 \text{ s}$$

$$721 \quad T_{m_2} = 2\pi \sqrt{\frac{m_2}{k_{cr}}} = 2\pi \sqrt{\frac{21517}{89865000}} = 0.097 \text{ s}$$

$$722 \quad \frac{T_m}{T_{m_2}} = \frac{1.77}{0.097} = 18.16 \text{ ; by using the design chart given in Fig. 13; } \gamma = 0.63$$

$$723 \quad \Delta = \gamma \times \frac{mv_0}{\sqrt{mk_{cr}(1 + \lambda_2)}} = 0.63 \times \frac{4683 \times 7}{\sqrt{4683 \times 89865000 \times (1 + 4.59)}} = 13.46 \text{ mm}$$

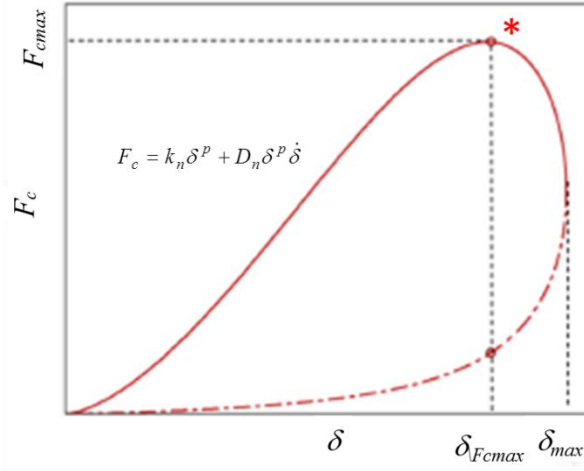
$$724 \quad \Delta_y = \frac{\phi_y h^2}{3} = \frac{0.0053125 \times 4.5^2}{3} = 36 \text{ mm}$$

725 It is concluded that:

726 $\Delta_y > \Delta$ meaning that the RC stem wall is predicted to respond within the limit of yield.

727 **Appendix B - derivation of the Eq. 15**

728 The non-linear force-displacement (F_c vs δ) relationship introduced by Eq. (15) is illustrated in
 729 Fig. 1 below.



730
 731 **Fig. B1 Peak contact force and maximum indentation in Hunt & Crossley Model**

732 When $\frac{\partial F}{\partial \delta} = 0$, the contact force F_c value reach to the peak value F_{cmax} as shown by Eq. (B1).

$$\frac{\partial F}{\partial \delta} = p k_n \delta^{p-1} + k_n (0.2p + 1.3) \frac{1 - COR}{COR} \frac{1}{\delta_o} \left(p \delta^{p-1} \dot{\delta} + \delta^p \frac{\partial \dot{\delta}}{\partial \delta} \right) = 0 \quad (B1)$$

733 By taking $x = \frac{\delta}{\delta_{max}}$ and $y = \frac{\dot{\delta}}{\delta_o}$ where δ_{max} is the maximum indentation, Eq. (B1) can be

734 simplified to Eq. B2 as shown below.

$$p + (0.2p + 1.3) \frac{1 - COR}{COR} \left(py + x \frac{\partial y}{\partial x} \right) = 0 \quad (B2)$$

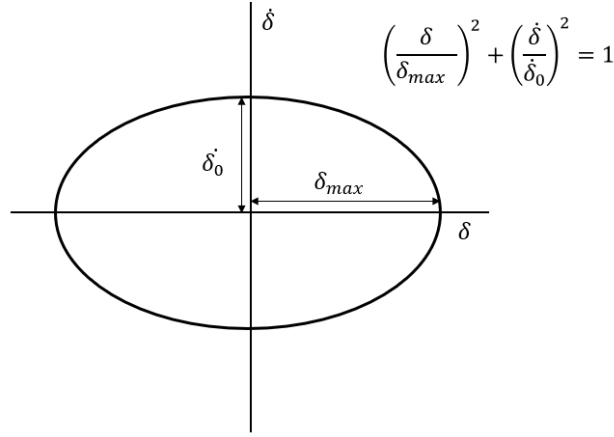
735 The elliptical relationship between indentation (δ) and its rate ($\dot{\delta}$) as illustrated in Fig. 2 is

736 adopted. Since $x^2 + y^2 = 1$, $\frac{\partial y}{\partial x}$ can be solved as shown in Eq. (B3)

$$\frac{\partial y}{\partial x} = \frac{1}{2} (-2x)(1 - x^2)^{-\frac{1}{2}} = -\frac{x}{\sqrt{1 - x^2}} = -\frac{\sqrt{1 - y^2}}{y} \quad (B3)$$

737 Substituting Eq. (B3) into (B2) and making use of the stated x-y relationship gives Eq. (B4).

$$py + (0.2p + 1.3) \frac{1 - COR}{COR} (py^2 - 1 + y^2) = 0 \quad (B4)$$



738

739 **Fig. B2 Adopted relationship of indentation with rate of indentation**

740 It can be shown by some algebraic manipulations that:

$$y^2 + \left(\frac{p}{(p+1)(0.2p+1.3)} \times \frac{COR}{1-COR} \right) y - \left(\frac{1}{p+1} \right) = 0$$

741 The root of the equation (y') can be expressed as shown in Eq. (B5):

$$y' = \frac{-b + \sqrt{b^2 + 4c}}{2} \quad \text{where } b = \frac{p \times COR}{(p+1)(0.2p+1.3)(1-COR)} \quad \text{and } c = \frac{1}{p+1} \quad (\text{B5})$$

742 The value of the peak contact force F_{cmax} may therefore be calculated using Eq. (B6).

$$F_{cmax} = k_n \left[1 + (0.2p + 1.3) \left(\frac{1 - COR}{COR} \right) y' \right] \times \delta_{max}^p \times [1 - y'^2]^{\frac{p}{2}} \quad (\text{B6})$$

743 where δ_{max}^p can be found using Eq. (B7) as shown in below. The derivation of Eq. (B7) is

744 available in Ref [51]. This is an improved version of Eq. (2) including COR and combined

745 target mass ratio.

$$\delta_{max}^p = \left(\frac{p+1}{2k_n} \left(\frac{\lambda_2}{1+\lambda_2} \right) m v_0^2 COR \right)^{\frac{p}{p+1}} \quad (\text{B7})$$

746 In summary, the value of F_{cmax} (Eq. (15)) may be calculated by combining the use of Eq. (B5),

747 Eq. (B6) and Eq. (B7).